Influences of triple junctions on stress-assisted grain boundary motion in nanocrystalline materials

Influences of triple junctions on stress-assisted grain boundary motion in nanocrystalline materials

Mohammad Aramfard and Chuang Deng

Department of Mechanical Engineering, University of Manitoba, 15 Gillson Street, Winnipeg, MB R3T 5V6, Canada

E-mail: dengc@ad.umanitoba.ca

Abstract

Stress-assisted grain boundary motion is among the most studied modes of microstructural evolution in crystalline materials. In this study, molecular dynamics simulations were used to systematically investigate the influences of triple junctions on the stress-assisted motion of symmetric tilt grain boundaries in Cu by considering a honeycomb nanocrystalline model. It was found that the grain boundary motion in nanocrystalline models was highly sensitive to the loading mode, and a strong coupling effect which was prevalent in bicrystal models was only observed when simple shear was applied. In addition, the coupling factor extracted from the honeycomb model was found to be larger and more sensitive to temperature change than that from bicrystal models for the same type of grain boundary under the same loading conditions. Furthermore, the triple junctions seemed to exhibit unusual asymmetric pinning effects to the migrating grain boundary and the constraints by the triple junctions and neighboring grains led to remarkable non-linear grain boundary motion in directions both parallel and normal to the applied shear, which was in stark contrast to that observed in bicrystal models. In addition, dislocation nucleation and propagation, which were absent in the bicrystal model, were found to play an important role on shear-induced grain boundary motion when triple junctions were present. In the end, a generalized model for shear-assisted grain boundary motion was proposed based on the findings from this research.

Keywords: shear coupling, grain boundary motion, triple junctions, molecular dynamics simulation

(Some figures may appear in colour only in the online journal)

1. Introduction

Stress-assisted grain boundary (GB) motion is the governing mechanism that leads to microstructural evolution in crystalline materials during loading and deformation [1–9]. In particular, translational GB motion coupled to a normal motion was considered to be the main mechanism responsible for the grain coarsening and plasticity in crystalline metals, i.e. under nanoindentation [10, 11], tension [4, 12–16] and shear [17, 18]. Based on a simple bicrystal model containing an isolated GB, Cahn and Taylor [19] have proposed the following equation to describe the pure coupled GB motion under applied shear stress:

$$v_{||} = \beta v_{\mathrm{n}} \tag{1}$$

where $v_{||}$ is the horizontal velocity parallel to the GB plane, v_{n} is the normal velocity perpendicular to the GB plane and β is the coupling factor. However, although the bicrystal models were successful in illustrating the fundamental GB motion mechanisms and can be used as good references to understand the behavior of realistic crystalline materials, the constraints on GB exerted by triple junctions (TJs) and neighboring grains need to be considered in order to satisfy the demanding interest in studying GB motion and microstructural evolution more physically especially in nanocrystalline (NC) metals; the volume fraction of TJs increases significantly as the grain size reduces to the nanometer scale [20].

In recent years some experimental works on stress-assisted GB motion have been reported [16, 21–29]. For example, Rupert *et al* have tested Al thin film under tensile stress and reported that the shear stress was the main reason for grain growth and GB migration in NC metals [28]. On the other hand, due to the complexity of GB networks in experimentally studied materials, theoretical analysis and atomistic simulations have been widely used as important alternatives to investigate the underlying mechanisms of GB motion in complex GB networks. For instance, Dynkin and Gutkin [30] and Bobylev *et al* [31] examined two types of TJs in symmetrical hexagonal and rectangular 2D grain networks and applied the disclination wedge theory to characterize the GB motion confined by TJs. They have shown that there was a strong dependence of GB migration on the geometry of TJs and the shear stress required for GB migration in a hexagonal grain was less than that in a rectangular one. Mesoscale simulations based on phase field [32–34], Monte Carlo [35–37] and network models [38] have also been used extensively to investigate grain growth. In particular, Zöllner [37] and Barrales-Mora *et al* [38] have used Monte Carlo Potts model and network models, respectively, to take into account the influence of TJs and quadruple lines on the grain growth in NC materials. However, severe limitations existed in these studies although they were important in evaluating the microstructural evolution in NC materials. For example, the analytical and mesoscale modeling would largely rely on the accuracy of important parameters such as boundary and junction mobility, which can only be fed from atomistic simulations. Furthermore, in the mesoscale studies by Zöllner [37] and Barrales-Mora *et al* [38], the influences of stress were not considered.

Some recent works taking into account the influences of TJs and neighboring grains have been done through molecular dynamics (MD) simulations [15, 39–43]. For example, Velasco *et al* [39] and Gianola *et al* [41] used a model consisting of a network of grains and applied strain controlled loading to investigate the stress-driven GB motion. They both showed that in spite of constraints such as TJs, the GB still migrated in a coupled fashion similar to that in bicrystal models but with a smaller coupling factor as compared to the theoretical value. However, a systematic examination on GB motion in a constrained environment is still lacking and some of the fundamental mechanisms remain to be revealed, e.g. how the GB motion would be influenced by neighboring moving GBs in realistic materials, how the GB becomes
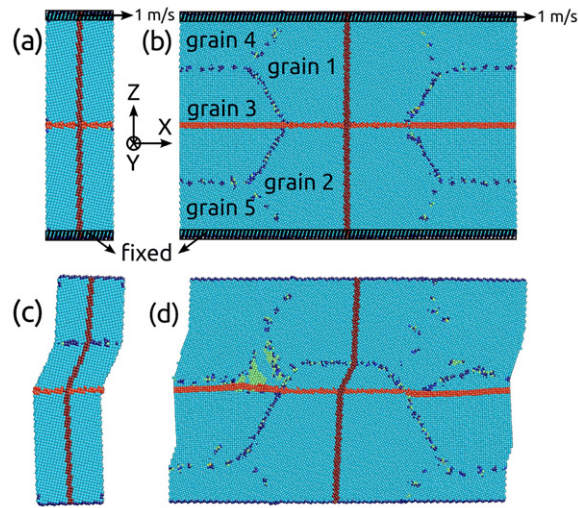
Figure 1. The schematic and atomistic configurations of (*a*) bicrystal and (*b*) NC models used in this work. Two slabs of atoms at the top and bottom of the models are fixed as rigid bodies. The shear is imposed by translating the upper slab at a constant velocity of $1\,\mathrm{m\,s^{-1}}$ while the lower slab is fixed. The horizontal and vertical marker lines are used to indicate the initial and instantaneous GB positions. The atomistic configurations of deformed (*c*) bicrystal and (*d*) NC models. The atom colors correspond to the local lattice orientation.

pinned and unpinned by the TJs and how the atomistic simulation results could validate or invalidate the theoretical models, etc.

The aim of this work is to systematically examine the stress-assisted GB motion in a complex GB network by MD simulations. For this purpose, two symmetric tilt GBs in Cu, $\Sigma 5$ and $\Sigma 17$, are constructed and simulated in a honeycomb model as shown in figure 1. In section 2, we describe the model and the methodology that we have used to simulate the GB motion. In section 3, we present the results in both types of GBs obtained at different temperatures and investigate the effects of TJs on the coupled GB motion in comparison with bicrystal models. In section 4, we explore the mechanisms of coupled GB motion involving TJ drag and pinning effects and compare it with the synthetic driving force method. The non-linear GB motion with the presence of TJs is also illustrated and discussed in this section and at last a generalized model describing the GB motion under shear in NC metals is proposed. Finally, the main findings of this work are summarized in section 5.

2. Methodology

Classical MD simulations were performed by using LAMMPS [44] with an embedded atom method potential for Cu [45]. The time step was 5 fs and each simulation ran up to a few nanoseconds. Two GB types, $\Sigma 5(1\,2\,0)$ and $\Sigma 17(3\,5\,0)$ with misorientation angles of $53.13°$ and $61.93°$ respectively, were constructed (e.g. the boundary between grain 1 and 2 in figure 1) for examination in both bicrystal and honeycomb NC models (referred as NC models). As shown in figure 1, the initial simulation cell was $\sim 30\,\mathrm{nm} \times 2.5\,\mathrm{nm} \times 20\,\mathrm{nm}$ in x, y and z directions (figure 1) and the GB to be studied was $\sim 11\,\mathrm{nm}$ along the x direction and confined by two identical TJs (the junctions between grains 1, 2 and 3). The lattice orientations for each

Table 1. Lattice orientations of individual grains as shown in figure 1 in $\Sigma 17$ NC model.

$\Sigma 17$	X	Y	Z
Grain 1	$[3\,\bar{5}\,0]$	$[0\,0\,\bar{1}]$	$[5\,3\,0]$
Grain 2	$[\bar{3}\,5\,0]$	$[0\,0\,1]$	$[5\,3\,0]$
Grain 3	$[1\,0\,0]$	$[0\,1\,0]$	$[0\,0\,1]$
Grain 4	$[1\,\bar{3}\,0]$	$[0\,0\,\bar{1}]$	$[3\,1\,0]$
Grain 5	$[1\,\bar{3}\,0]$	$[0\,0\,1]$	$[\bar{3}\,\bar{1}\,0]$

Table 2. Lattice orientations of individual grains as shown in figure 1 in $\Sigma 5$ NC model.

$\Sigma 5$	X	Y	Z
Grain 1	$[1\,\bar{2}\,0]$	$[0\,0\,\bar{1}]$	$[2\,1\,0]$
Grain 2	$[\bar{1}\,2\,0]$	$[0\,0\,1]$	$[2\,1\,0]$
Grain 3	$[1\,0\,0]$	$[0\,1\,0]$	$[0\,0\,1]$
Grain 4	$[1\,\bar{5}\,0]$	$[0\,0\,\bar{1}]$	$[5\,1\,0]$
Grain 5	$[1\,\bar{5}\,0]$	$[0\,0\,1]$	$[\bar{5}\,\bar{1}\,0]$

grain in the NC model were listed in tables 1 and 2 for $\Sigma 17(3\,5\,0)$ and $\Sigma 5(1\,2\,0)$, respectively. In all models, periodic boundary conditions were applied along x and y directions while the z direction was set free. Prior to any deformation, the models were relaxed at the desired temperature for 100 ps at zero pressure under NPT (isothermal, isobaric) using the Nosé–Hoover thermostat [46, 47].

In order to apply shear deformation, atoms within two thin slabs at the top and bottom of the models were fixed. The upper slab was moved as a rigid body at a constant velocity of $1\,\mathrm{m\,s^{-1}}$ in the x direction (parallel to the GB plane), while the lower slab remained fixed. During the shear deformation, canonical (NVT) thermostat was applied to the models excluding the two thin slabs. For comparison purposes, the synthetic driving force method developed by Janssens *et al* [48] was also used to study the GB motion in both bicrystal and NC models. A driving force of 0.01 eV (equivalent to $\sim$0.14 GPa) was applied, similar to that used by Homer *et al* [49].

Horizontal and vertical marker lines were used to keep track of the GB motion in normal and tangential directions to the GB plane (figure 1). For each GB type at any desired temperature, one simulation was performed for the bicrystal model but four simulations with different initial thermo conditions were performed for the NC model. The atomistic configuration of each model was visualized by AtomEye [50].

3. Results

3.1. Shear-coupled GB motion in NC models

In order to investigate the influences of TJs and neighboring grains on shear-induced GB motion, the GB motion in both bicrystal and NC models (figure 1) under identical shear deformation was studied and compared at various temperatures ranging from 200 to 800 K. As shown in figures 1(*c*) and (*d*), the path of GB motion can be tracked by the horizontal and vertical marker lines; the horizontal marker was to indicate the initial GB position and the vertical marker was to indicate the instantaneous GB position and the path that the GB has
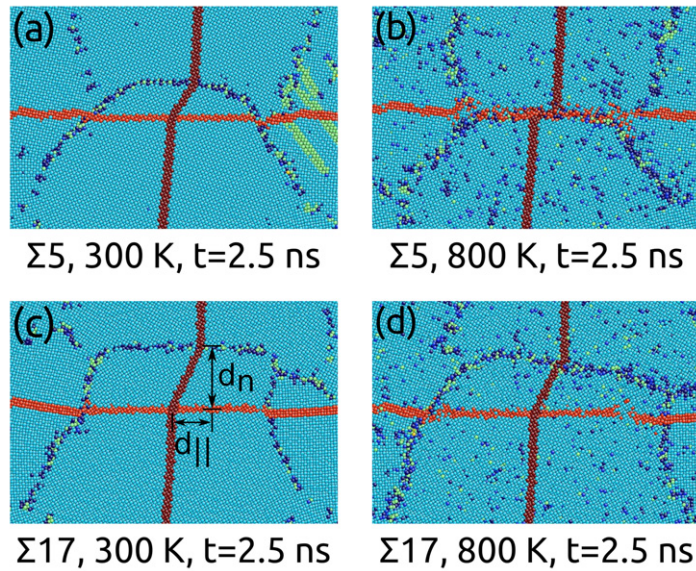
Figure 2. Atomistic configurations of NC models for deformed $\Sigma 5$ GB at (*a*) 300 K and (*b*) 800 K and $\Sigma 17$ GB at (*c*) 300 K and (*d*) 800 K, respectively, after $t = 2.5$ ns. The atom colors correspond to the local lattice orientation.

traveled. In spite of TJs and neighboring grains, the GB still showed a shear-coupled motion (figure 1(*d*)), which was consistent with previous studies by Velasco *et al* [39] and Gianola *et al* [41]. Moreover, the instantaneous coupling factor β can be computed from the slope of the inclined vertical marker. By comparing figures 1(*c*) and (*d*), it was found that the TJs had a strong pinning effect to the GB plane which would potentially hinder the GB motion. It is also important to note in figure 1(*d*) that the GB became curved due to this pinning effect. As has been reported from previous experiments and MD simulations [51, 52], the curved interface could induce a drag force in the opposite direction to the GB motion, which could also potentially affect the shear coupling factor. Furthermore, while no dislocations were observed in the bicrystal model, dislocation nucleation was found near TJs in the NC model. We will discuss the influence of the dislocations on the TJ and GB motion in section 4.4.

3.2. Temperature effect on shear-coupled GB motion

It has been reported by Cahn *et al* [53] and Homer *et al* [49] based on the bicrystal models that temperature played an important role in the shear-coupled GB motion. To explore the temperature effect on shear-induced GB motion when TJs were present, we varied the temperature from 200 to 800 K with an increment of 100 K in the NC models. Figures 2(*a*) and (*b*) show the deformed $\Sigma 5$ NC model after 2.5 ns at 300 K and 800 K, respectively. It can be seen from figure 2(*b*) that at 800 K, the confined $\Sigma 5$ GB showed almost complete sliding with no coupled normal motion. In contrast, no sliding was observed for the $\Sigma 5$ GB in bicrystal model at 800 K, which agreed with Cahn *et al* that the $\Sigma 5(1\,2\,0)$ GB in bicrystal model did not slide until the temperature reached 1000 K [53]. This finding was in contrast to the work by Bernstein [54] who depicted that constrained GB showed less sliding and relevant grains did not show much rotation in compare with unconstrained GB, i.e. in bicrystal models. On the other hand, the $\Sigma 17$ GB showed no sliding behavior at temperatures up to 800 K in either
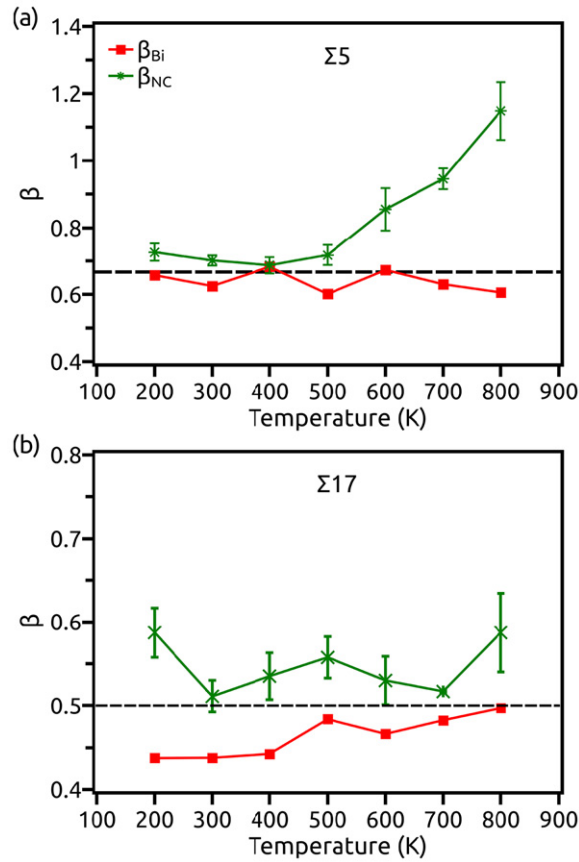
Figure 3. Coupling factor β at different temperatures in NC and bicrystal models containing (a)$\Sigma 5$ and (b)$\Sigma 17$ GBs. The horizontal dashed lines show the theoretical values of β for the corresponding GB type.

bicrystal or NC models. Additionally, figures 2(c) and (d) showed that the $\Sigma 17$ GB in NC model moved in a similar fashion at 300 and 800 K, suggesting that the shear-coupled motion of $\Sigma 17$ GB had no significant temperature dependence.

Some other differences were also observed by inspecting the TJs and GB in both $\Sigma 5$ and $\Sigma 17$ NC models. At 300 K, the TJs showed a strong pinning effect in the $\Sigma 5$ NC model, which resulted in significant curvature of the GB and dislocation nucleation. In the $\Sigma 17$ NC model, however, the TJs at both ends of the GB moved along with the GB and no significant curvature of the GB plane was caused.

To quantitatively illustrate the temperature effects on the coupling factor in the shear deformed NC model, the horizontal and normal movements at the center of the GB were analyzed (figure 2(c)$d_{\parallel}$ and d_{n}, respectively). The results are plotted in figures 3(a) and (b) for $\Sigma 5$ and $\Sigma 17$ GBs, respectively for both bicrystal (red) and NC (green) models under shear deformation. The error bars were based on four sets of simulations at each temperature for the NC models. The horizontal dashed lines marked the theoretical predictions of β for each type of GB; the theoretical value of β is 0.667 for $\Sigma 5$ GB and 0.5 for $\Sigma 17$ GB, respectively [19]. While Velasco *et al* [39] and Schäfer *et al* [40] have both reported β to be smaller than the theoretical predictions or that obtained from simple bicrystal models, the computed β in NC models with

TJs, however, was higher than theoretical anticipations [19] and bicrystal results [53] for both $\Sigma 5$ and $\Sigma 17$ GBs. The dramatic difference between current and previous studies may mainly originate from the different loading conditions. In this study, shear deformation was applied by rigidly moving two thin slabs in the direction parallel to the GB plane [53], while in [39, 40] the deformation was applied by applying uniaxial tension to a model consisting of randomly distributed grains. Further discussion about the cause of the seemingly large coupling factor under the shear deformation applied in the current study can be found in sections 4.1 and 4.2.

Another interesting phenomenon in figure 3(*a*) is that while the coupling factor of $\Sigma 5$ GB in bicrystal models remained almost constant around the theoretical value at all temperatures, the β of $\Sigma 5$ GB in NC models increased sharply when the temperature increased from 500 to 800 K. The increase in β of $\Sigma 5$ GB in NC models was mainly caused by GB sliding (as shown in figure 2(*b*)), which became more pronounced at higher temperatures. In $\Sigma 17$ NC model, on the other hand, there was no overall trend of change in β when temperature varied. Nevertheless, slightly larger β was observed at 200 and 800 K as compared to other temperatures in the $\Sigma 17$ NC model, which was caused by the curvature in GB during the migration.

3.3. Time dependent non-linear GB motion

In sharp contrast to the observations from bicrystal models [53], it was interesting to find that the GB did not move at a constant velocity in directions either tangential or normal to the GB in the NC models (figure 4). In spite of the fact that the shear deformation was applied by translating the top layer of atoms at a constant velocity of $1 \, \mathrm{m \, s^{-1}}$, as shown in figure 4 ($\Sigma 5$ GB at 600 K in figure 4(*a*) and $\Sigma 17$ GB at 200 K in figure 4(*b*), respectively), the GBs in NC models moved in an accelerated fashion in directions both parallel and normal to the applied shear. The non-linear behavior shown in figure 4 indicated that in realistic crystalline materials the shear-induced GB motion could be dramatically different from the constant value that has been assumed in the idealized bicrystal models.

4. Discussion

4.1. Effect of loading mode on coupling factor β

It was shown in figure 3 that the coupling factor β in NC models is generally higher than that in bicrystal models, which is contrary to the observations by Velasco *et al* [39] and Schäfer and Albe [40] that β in NC models was lower than that in bicrystal models. The main reason for this discrepancy might be the different loading modes that have been used in these studies as mentioned earlier. In order to further investigate the influence of loading mode on the coupling factor, we performed simulations on both bicrystal and NC models using the synthetic driving force method [48]. Excess energy of $-0.01 \, \mathrm{eV/atom}$ (equivalent to 0.14 GPa) was artificially added to the lower grain in bicrystal and grain 2 in NC models, respectively. Subsequently the grain with lower energy tended to coarsen and its GBs moved outward. The normal positions of the GB in both bicrystal and NC models for both GB types were computed and are shown in figure 5. Figure 5(*a*) is the plot of GB displacement in both bicrystal and NC models for $\Sigma 5$. Comparing figures 5(*a*) and (*b*) it is noteworthy that the GBs in bicrystal and NC models behaved very differently. In bicrystal models of both GB types, the GBs moved significantly faster than in NC models. On the other hand, while the $\Sigma 5$ GB moved more sluggishly than the $\Sigma 17$ GB in bicrystal models, the $\Sigma 5$ GB moved much further than the $\Sigma 17$ GB in NC models. The difference is likely due to the strength of the respective TJs that retarded the GB. Another interesting result is that the $\Sigma 5$ GB in both models moved with a stick-slip behavior
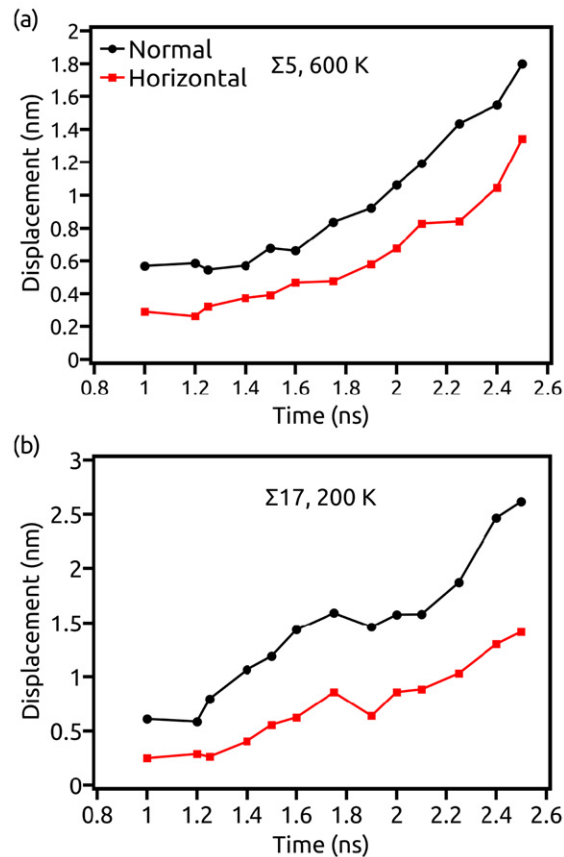
Figure 4. Horizontal and normal displacements as a function of time for (*a*) $\Sigma 5$ at 600 K and (*b*) $\Sigma 17$ GBs at 200 K in NC models.

while $\Sigma 17$ models moved smoothly. This observation is consistent with findings based on bicrystal models from Cahn *et al* [53], who found that it is more difficult for $\Sigma 5$ GB to move than $\Sigma 17$ GB due to an applied shear. Specifically, Cahn *et al* [53] found that $\Sigma 5(2\,1\,0)$ GB (the same GB as studied in current NC models) would experience a period of waiting time before a sudden move of the GB could occur, which corresponded to the point when the shear stress reached a threshold. The shear stress acting on the GB, however, would drop immediately after the sudden move of the GB so that another round of waiting started. The cycle consisting of sudden GB motion and waiting would repeat during the shear-coupled GB motion, causing the so called 'stick-slip' behavior. In contrast, the $\Sigma 17(5\,3\,0)$ GB was found to move spontaneously as long as the shear was applied, resulting in a relatively smooth GB motion both horizontally and vertically [53].

Furthermore, figure 5(*c*) clearly shows the effect of the loading mode on coupling factor. Unlike the shear-induced GB motion, the GB did not show significant coupling and in some cases almost pure normal motion was observed in NC models regardless of the driving force applied. While the coupling factor β has been claimed to be a pure geometry factor based on simple bicrystal models, which has been found to be independent of the loading mode [49, 53], it is important to find out that the coupling in NC models with TJs can be significantly influenced by how the model is deformed according to current and previous MD studies [39–41].
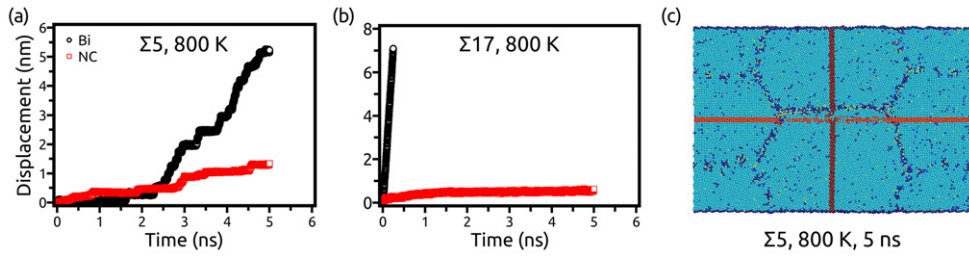
Figure 5. Normal displacement of bicrystal and NC models for (*a*) Σ5 and (*b*) Σ17 GBs at 800 K. (*c*) Atomic configuration of Σ5 NC model at 800 K after 5 ns. The atom colors correspond to the local lattice orientation.
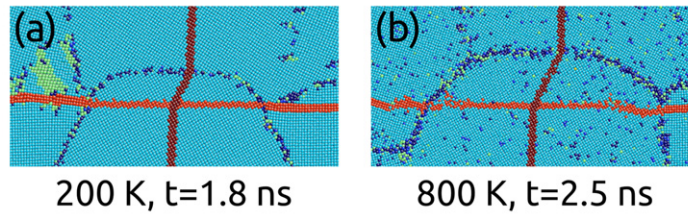

Figure 6. Curved GB in Σ17 NC model (*a*) after 1.8 ns at 200 K and (*b*) after 2.5 ns at 800 K. The atom colors correspond to the local lattice orientation.

4.2. Influences of TJ pinning on the coupling factor

Besides the loading mode and the geometry of the GB itself, there are some other factors that might influence the coupling factor in NC models. It was shown in figure 3 that generally the deviation of coupling factor from theoretical predictions was more severe in the Σ5 NC model than in the Σ17 NC model, which can be attributed to the different pinning effects of TJs in these two models.

In Σ17 NC model the deviation of coupling factor from the theoretical anticipation and the bicrystal model was relatively small; noticeable deviations were observed only at 200 and 800 K. By examining the atomistic configurations, we found significant pinning effects of TJs in Σ17 NC models only at 200 and 800 K; the Σ17 GB was significantly curved during the coupled GB motion only at 200 K (figure 6(*a*)) and 800 K (figure 6(*b*)), while at other temperatures the GB remained relatively flat at all times (compare with figure 2(*c*)). On the other hand, strong pinning effects and a severely curved GB were observed in Σ5 NC models at almost all temperatures smaller than 700 K; some examples were shown in figure 1(*d*) and figure 2(*a*). The dramatic difference between the two NC models indicated that it was more difficult for the Σ5 GB to move as compared to the Σ17 GB, which can be attributed to the 'stick-slip' GB motion in Σ5 NC models and relatively smooth GB motion in Σ17 NC models as shown in figure 5. As has been discussed in section 4.1, Σ5 GB would move only if a threshold stress was reached, while Σ17 GB would move spontaneously as long as the shear was applied.

It has been shown that the curved interface would impose a strong force [51, 52] in the direction against the normal GB motion. Consequently, the strong pinning effects from TJs would result in reduced normal GB velocity and accordingly an increased coupling factor, as shown in figure 3. It should be noted here that to measure the normal GB displacement

in NC models, we used the marker in such a way that when the GB was curved, the normal displacement of the center point of the GB was measured. Therefore, the normal velocity of a curved GB used to compute was dramatically higher than that averaged over the entire GB. A larger deviation in the coupling factor from the theoretical predictions would thus be expected by considering an average normal GB velocity in NC models.

4.3. Cause of non-linear GB motion in NC models during shear deformation

To compute β in bicrystal models, it was assumed that the shear imposed on the top of the model was equal to the shear acting on the GB plane [53]. Thus the horizontal velocity of the top slab was assumed to be the same as the horizontal GB velocity ($v_{\parallel}$ in equation (1)). To validate this assumption in NC models, the shear deformation at different locations along the z direction in grain 1 (as defined in figure 1(*b*)) was analyzed by tracking the horizontal motion of four different layers between the GB plane and the top surface (inset of figure 7(*a*)). The horizontal displacement versus time of the four different layers was plotted in figure 7 for Σ17 GB at 300 and 800 K. For comparison, the same analysis was performed for Σ17 GB in bicrystal models and plotted in the inset of figure 7(*b*). The results from bicrystal models showed that the assumption of constant shear in the top grain by translating the top slab at a constant velocity was accurate (inset in figure 7(*b*)). On the contrary, the results based on NC models showed that this assumption cannot be applied to NC models with TJs; both figures 7(*a*) and (*b*) show that the horizontal velocity of atom layers in grain 1 was higher at locations closer to the top surface. Furthermore, it was found that the differences in horizontal velocities among the four layers increased dramatically as the temperature dropped from 800 to 300 K. It is thus hinted that the influences on shear-coupled GB motion due to the constraints by TJs and the neighboring grains were more pronounced at lower temperatures.

Since in NC models the horizontal translation of the top slab cannot result in a uniform shear across the top grain as in bicrystal models, the non-linear GB motion as shown in figure 4 can be well explained. Specifically, the magnitude of shear imposed on the GB plane depended on its vertical location which increased as the GB approached the top surface.

To explain this behavior, we show in figure 8 the atomistic configuration of a deformed Σ17 NC model at 200 K. It is noted that in almost all the studied NC models, more than one GB would move due to the shear coupling effects. In the model presented in figure 8, the Σ17 GB between grains 1 and 2 moved upward in a coupled manner and dragged grain 1 to the right while the GB between grains 3 and 4 (refer to figure 1) moved downward and dragged grain 4 to the left also in a coupled manner. The two arrows indicate the moving paths of the two GBs. Such collective motion of GB networks resulted in a dragged horizontal motion of top layer and consequently non-uniform shear in grain 1.

It is important to mention that this non-uniform shear deformation and non-linear GB motion was unique in NC models when confinements by TJs and neighboring GBs were present and cannot be seen in unconfined models. Since in realistic materials with complex GB networks such confinements are prevalent, the results from this study should stimulate further experimental investigations on shear-induced non-linear GB motion.

4.4. Influences of dislocation on GB and TJ motion

Besides the non-uniform shear in NC models, figure 7 shows a peculiar 'jump' behavior during the shear-induced GB motion as indicated by the vertical dashed line. It was also found that the 'jump' became more noticeable at 300 K than at 800 K. To understand the mechanisms that caused the 'jump', the atomistic configurations of the NC models before and after the 'jump'
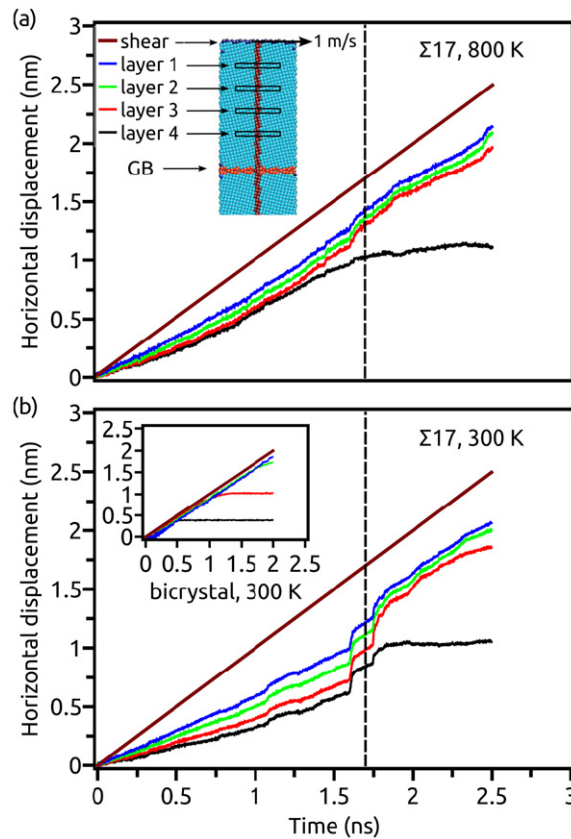
Figure 7. Horizontal displacement versus time of four different layers of atoms above the GB in the Σ17 NC model at (*a*) 800 K and (*b*) 300 K. The vertical dashed lines indicate the time at which a 'jump' in GB displacement occurred. The inset in (*a*) shows the schematic of the four layers at different locations between the GB plane and the top surface. The inset in (*b*) shows the horizontal displacement versus time of the same four layers in the bicrystal Σ17 model at 300 K.

were analyzed. In figures 9(*a*) and (*b*), four snapshots showing the GB motion in the Σ5 NC model at 200 K during the 'jump' from 2.7 to 3.1 ns and four snapshots showing the GB motion in the Σ17 NC model at 300 K from 1.7 to 2.05 ns, respectively, are presented; the TJs were highlighted by the dashed circles.

In figure 9(*a*) at $t = 2.7$ ns no dislocations were observed, but 0.1 ns later, dislocations appeared near both the left and right TJs and at $t = 3.05$ ns, a clear 'jump' of the right TJ can be seen, which was accompanied by the disappearance of dislocations. Finally, all the dislocations disappeared at $t = 3.1$ ns.

In figure 9(*b*), it can be seen that at $t = 1.7$ ns, like in Σ5 model, there were no dislocations, after 0.15 ns ($t = 1.85$ ns) some dislocations appeared near both the left and right TJs. During this process, the left TJ moved upwards while the right TJ remained pinned. Furthermore, the dislocation near the right TJ disappeared at $t = 1.9$ ns and the right TJ jumped up, implying that the TJ 'jump' and dislocation activity were correlated. Although the time change during this happening was very short (only 0.05 ns), the GB moved substantially, which led to the 'jump'
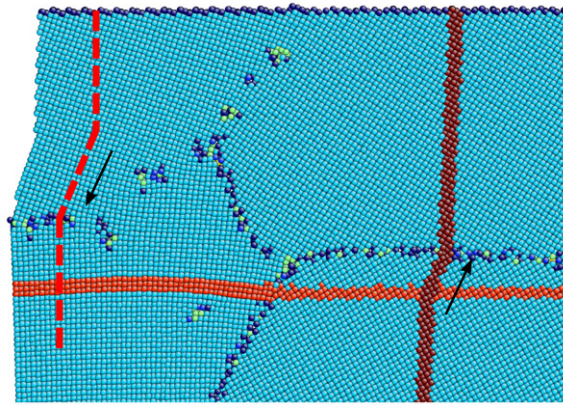
Figure 8. Shear induced motion of different GBs in the $\Sigma 17$ NC model at 200 K. The arrows indicate the moving paths of the two GBs.
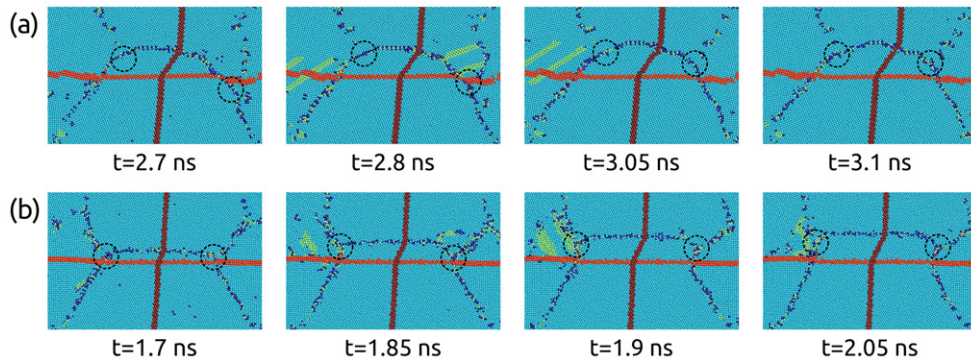

Figure 9. Atomistic configurations of (*a*) $\Sigma 5$ NC model at $t = 1.7$, 1.85, 1.9 and 2.05 ns and (*b*) $\Sigma 17$ NC model at $t = 1.7$, 1.85, 1.9 and 2.05 *ns* at 300 K. The positions of TJs are highlighted by the dashed circles. The atom colors correspond to the local lattice orientation.

observed in figure 7. On the other hand, the accompanied dislocation activities suggested that the TJs were relatively immobile as compared to the GB under the applied shear, which was the cause of the strong pinning effect by TJs. Finally, at $t = 2.05$ ns, the GB became almost flat and the dislocation on the right side disappeared completely. Dislocation on the left side also faded quickly as the shear deformation continued. This dislocation activity is inconsistent with what Legros *et al* observed in NC Al thin film [16]. They reported that dislocation activities would follow the grain growth. It can be concluded that the dislocation activities seen in the NC models were due to restrictions from TJs and the neighboring grains; no dislocation nucleation was observed in the bicrystal models.

4.5. Asymmetric pinning effects of TJs and generalized stress-assisted GB motion mode in NC materials

By reviewing some of the atomistic figures in NC models of both types of GBs that we have studied, it can be found that there is an asymmetric behavior in the two TJs that confined the
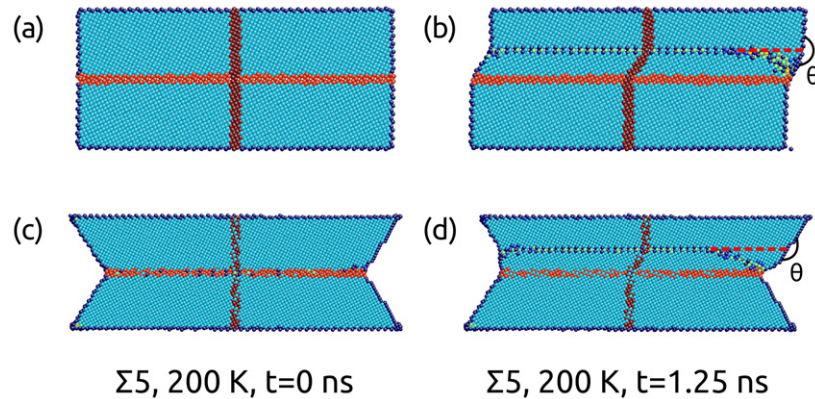
Figure 10. Atomistic configurations of Σ5 bicrystal models at 200 K (*a*), (*c*) undeformed and (*b*), (*d*) deformed after 1.25 ns. Dashed red lines show the GB position if it was completely flat. The atom colors correspond to the local lattice orientation.

GB, e.g. one TJ would become unpinned earlier than the other one (for example, figures 2(*d*), 6(*b*) and 9). To understand the underlying mechanism of the pinning and unpinning of TJs that led to this asymmetry we built two bicrystal models with free surface conditions in the *x* direction (figure 10) and applied shear deformation similar to what we did in NC and bicrystal models with periodic conditions. Figures 10(*a*) and (*c*) show the undeformed configurations of these models with flat and inclined free surfaces, respectively, to ensemble TJs in NC materials with different geometries. The GB type is symmetric Σ5 and the simulations were performed at 200 K. After 1.25 ns whereas the GB moved both horizontally and vertically due to the coupling effects, the two ends of GB in both models which were similar to the TJs in NC models showed asymmetric behavior similar to that found in figure 9; the left end moved along with GB while the right end was less mobile and pinned. Such asymmetry caused the GB to curve at the right end (the red dashed line shows the hypothetical GB position if it was not curved), which might be due to the fact that if the right end also moved along with the GB, one of the angles constructed in it (θ in figures 10(*b*) and (*d*)) would become critically larger than the equilibrium angle, i.e. 120° while the two other angles were much smaller. To avoid this level of eccentricity and minimize the energy, the right end tended to pin and made the three angles closer to 120°. The same mechanism should have been involved with the asymmetric TJ motion in NC models mentioned earlier. It would be expected that the asymmetric pinning of the two TJs on GB motion would produce more pronounced effects at relatively smaller grain sizes, although more simulations need to be performed in the future to validate it.

Based on all the atomistic mechanisms found above, we propose a four-step model to generalize the stress-assisted GB and TJ motion in a hexagonal geometry under shear deformation (figure 11). By applying shear parallel to a GB plane confined by two hexagonal TJs at the two ends, GB tends to move upward first (or downward based on the GB geometry) but the TJs are pinned and do not move at the very beginning. The result is a curved GB as shown in figure 11(*b*). Due to the asymmetric nature of the TJs, the left TJ moves easier than the right TJ which results in the unpinning of the left TJ to catch up with the GB by a 'jump', as shown in figure 11(*c*). Finally, after enough shear stress or energy has been accumulated in the right TJ, it will eventually move along and catch up with GB also by a 'jump', as shown in figure 11(*d*). In comparison with the model proposed by Bobylev *et al* [31], the model in figure 11 depicts the intermediate steps that fill the gap between the initial and final states of the moving GB
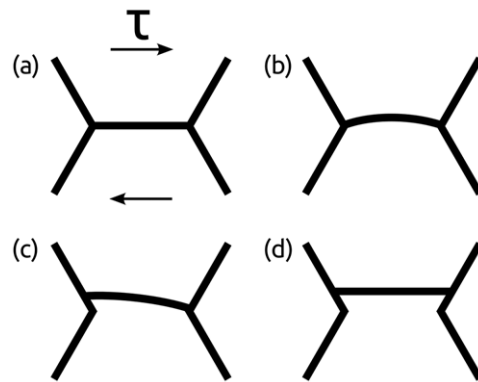
Figure 11. Generalized model explaining the GB and TJ motion under shear in NC materials. (*a*) Initial configuration, (*b*) both TJs are pinned causing the GB to curve, (*c*) left TJ is unpinned and (*d*) both the TJs become unpinned and catch up with the GB.

in an NC model. We would like to mention that the proposed model was based on only two special symmetric GBs. While this choice was made so that a direct comparison to past studies would be straightforward and the influences of TJs could be highlighted, asymmetric and non-sigma GBs [55] should also be studied in the future to validate this model. Nevertheless, while the misorientation angles are close, the two symmetric tilt GBs studied in this work are representative of the typical GB behavior that has been found in the past based on shear-coupled GB motion in the bicrystal models. For example, $\Sigma5$ GB is representative of the group of GBs that show stick-slip motion and $\Sigma17$ GB is representative of the group of GBs that show spontaneous motion [53]. As a result, we would not expect the conclusions to be significantly different if much more different misorientation angles are considered.

It is worth mentioning that the four-step model agrees qualitatively with TEM investigations on stress-assisted GB motion [16]. For instance, Legrosa *et al* [16] have observed fast GB motion in stressed Al NC thin film through *in situ* TEM investigation and found that a grain could grow locally by the motion of just a portion (the upper right) of the GB to form a 'nose'. This is a strong indication that it is possible to have non-uniform motion of different parts of the same GB, which can be well depicted by the schematic shown in figure 11(*c*).

5. Conclusions

Stress-assisted motion of two different types of GBs in Cu with the presence of TJs and neighboring grains in NC models has been simulated by MD. The influences of TJs and temperature on GB motion have been systematically investigated. Overall, the following conclusions can be made from this work:

- The loading mode has a huge influence on shear-coupled GB motion when TJs are present and the same GB may exhibit dramatically different coupling effects under different loadings.
- Under simple shear, the coupling factor in NC models is higher than that in bicrystal models due to the pinning effects from TJs, which result in severe GB curvature and drag against normal GB motion.
- The dependence of shear-coupled GB motion on temperature is significantly stronger in NC models than in bicrystal models especially for $\Sigma5$ GB. In particular, pure GB sliding has been found in $\Sigma5$ NC models at 800 K.

- Remarkable non-linear horizontal and normal GB motion is prevalent in NC models, which is in stark contrast to that in bicrystal models where GB generally moves at a constant velocity under the shear deformation applied in this study. The cause of non-linearity in GB motion is related to the non-uniform shear deformation in the grain due to the collective motion of other GBs in the NC system.
- The TJs have asymmetric pinning effects on the GB motion in NC models and dislocation activities have been found to accommodate TJ motion and play a role on GB motion under the applied shear.
- A generalized model is proposed on shear stress-induced GB motion in hexagonal NC models.

This study should stimulate relevant experimental work and shed light on the comprehensive understanding of stress-induced GB motion in realistic materials.

Acknowledgments

References

[1] Sutton A P and Balluffi R W 1995 *Interfaces in Crystalline Materials* (Oxford: Clarendon)
[2] Wolf D, Yamakov V, Phillpot S R, Mukherjee A and Gleiter H 2005 Deformation of nanocrystalline materials by molecular-dynamics simulation: relationship to experiments? *Acta Mater.* **53** 1–40
[3] Yamakov V, Wolf D, Phillpot S R, Mukherjee A K and Gleiter H 2003 Deformation-mechanism map for nanocrystalline metals by molecular-dynamics simulation *Nature Mater.* **3** 43–7
[4] Dao M, Lu L, Asaro R J, De Hosson J T M and Ma E 2007 Toward a quantitative understanding of mechanical behavior of nanocrystalline metals *Acta Mater.* **55** 4041–65
[5] Schiøtz J and Jacobsen K W 2003 A maximum in the strength of nanocrystalline copper *Science* **301** 1357–9
[6] Zhang K, Weertman J R and Eastman J A 2005 Rapid stress-driven grain coarsening in nanocrystalline Cu at ambient and cryogenic temperatures *Appl. Phys. Lett.* **87** 061921
[7] Li C H, Edwards E, Washburn J and Parker E 1953 Stress-induced movement of crystal boundaries *Acta Metall.* **1** 223–9
[8] Van Swygenhoven H, Derlet P M and Hasnaoui A 2002 Atomic mechanism for dislocation emission from nano-sized grain boundaries *Phys. Rev. B* **66** 024101
[9] Schiøtz J, Di Tolla F D and Jacobsen K W 1998 Softening of nanocrystalline metals at very small grain sizes *Nature* **391** 561–3
[10] Aifantis K E and Ngan A H W 2007 Modeling dislocation–grain boundary interactions through gradient plasticity and nanoindentation *Mater. Sci. Eng. A* **459** 251–61
[11] Jin M, Minor A M, Stach E A and Morris J W Jr 2004 Direct observation of deformation-induced grain growth during the nanoindentation of ultrafine-grained Al at room temperature *Acta Mater.* **52** 5381–7
[12] Sharon J A, Su P-C, Prinz F B and Hemker K J 2011 Stress-driven grain growth in nanocrystalline Pt thin films *Scr. Mater.* **64** 25–8
[13] Van Swygenhoven H and Derlet P M 2001 Grain-boundary sliding in nanocrystalline fcc metals *Phys. Rev. B* **64** 224105
[14] Badirujjaman S, Li X-W and Winning M 2007 Motion of [1 0 0]-tilt grain boundaries under cyclic stresses *Mater. Sci. Eng. A* **448** 242–8

[15] Sansoz F and Dupont V 2006 Grain growth behavior at absolute zero during nanocrystalline metal indentation *Appl. Phys. Lett.* **89** 111901

[16] Legros M, Gianola D S and Hemker K J 2008 *In situ* TEM observations of fast grain-boundary motion in stressed nanocrystalline aluminum films *Acta Mater.* **56** 3380–93

[17] Bainbridge D W, Choh H L and Edwards H E 1954 Recent observations on the motion of small angle dislocation boundaries *Acta Metall.* **2** 322–33

[18] Molodov D A, Gorkaya T and Gottstein G 2011 Dynamics of grain boundaries under applied mechanical stress *J. Mater. Sci.* **46** 4318–26

[19] Cahn J W and Taylor J E 2004 A unified approach to motion of grain boundaries, relative tangential translation along grain boundaries, and grain rotation *Acta Mater.* **52** 4887–98

[20] Meyers M A, Mishra A and Benson D J 2006 Mechanical properties of nanocrystalline materials *Prog. Mater. Sci.* **51** 427–556

[21] Czubayko U, Sursaeva V G, Gottstein G and Shvindlerman L S 1998 Influence of triple junctions on grain boundary motion *Acta Mater.* **46** 5863–71

[22] Protasova S, Gottstein G, Molodov D, Sursaeva V and Shvindlerman L 2001 Triple junction motion in aluminum tricrystals *Acta Mater.* **49** 2519–25

[23] Gottstein G and Shvindlerman L S 2013 Grain boundary junctions, ridges and facets: their kinetics and effects on grain microstructure evolution *Emerg. Mater. Res.* **2** 71–8

[24] Saldana C, Murthy T G, Shankar M R, Stach E A and Chandrasekar S 2009 Stabilizing nanostructured materials by coherent nanotwins and their grain boundary triple junction drag *Appl. Phys. Lett.* **94** 021910

[25] Mattissen D, Molodov D A, Shvindlerman L S and Gottstein G 2005 Drag effect of triple junctions on grain boundary and grain growth kinetics in aluminium *Acta Mater.* **53** 2049–57

[26] Gianola D S, Eberl C, Cheng X M and Hemker K J 2008 Stress-driven surface topography evolution in nanocrystalline Al thin films *Adv. Mater.* **20** 303–8

[27] Gianola D S, Van Petegem S, Legros M, Brandstetter S, Van Swygenhoven H and Hemker K J 2006 Stress-assisted discontinuous grain growth and its effect on the deformation behavior of nanocrystalline aluminum thin films *Acta Mater.* **54** 2253–63

[28] Rupert T J, Gianola D S, Gan Y and Hemker K J 2009 Experimental observations of stress-driven grain boundary migration *Science* **326** 1686–90

[29] Merkle K L, Thompson L J and Phillipp F 2004 *In-Situ* HREM studies of grain boundary migration *Interface Sci.* **12** 277–92

[30] Dynkin N K and Gutkin M Y 2012 Migration of grain boundaries in free-standing nanocrystalline thin films *Scr. Mater.* **66** 73–6

[31] Bobylev S V and Ovid'ko I A 2009 Mobility of triple junctions of grain boundaries during their migration in deformed nanocrystalline materials *Rev. Adv. Mater. Sci.* **22** 39–51

[32] Darvishi Kamachali R and Steinbach I 2012 3-D phase-field simulation of grain growth: topological analysis versus mean-field approximations *Acta Mater.* **60** 2719–28

[33] Krill Iii C E and Chen L-Q 2002 Computer simulation of 3-D grain growth using a phase-field model *Acta Mater.* **50** 3059–75

[34] Moelans N, Blanpain B and Wollants P 2008 Quantitative analysis of grain boundary properties in a generalized phase field model for grain growth in anisotropic systems *Phys. Rev. B* **78** 024113

[35] Potts R B 1952 Some generalized order-disorder transformations *Math. Proc. Camb. Phil. Soc.* **48** 106–9

[36] Yu Q and Esche S K 2003 Three-dimensional grain growth modeling with a Monte Carlo algorithm *Mater. Lett.* **57** 4622–6

[37] Zöllner D 2011 A Potts model for junction limited grain growth *Comput. Mater. Sci.* **50** 2712–9

[38] Barrales-Mora L A, Gottstein G and Shvindlerman L S 2012 Effect of a finite boundary junction mobility on the growth rate of grains in two-dimensional polycrystals *Acta Mater.* **60** 546–55

[39] Velasco M, Van Swygenhoven H and Brandl C 2011 Coupled grain boundary motion in a nanocrystalline grain boundary network *Scr. Mater.* **65** 151–4

[40] Schäfer J and Albe K 2012 Competing deformation mechanisms in nanocrystalline metals and alloys: coupled motion versus grain boundary sliding *Acta Mater.* **60** 6076–85

[41] Gianola D S, Farkas D, Gamarra M and He M 2012 The role of confinement on stress-driven grain boundary motion in nanocrystalline aluminum thin films *J. Appl. Phys.* **112** 124313

[42] Gottstein G and Shvindlerman L S 2005 Grain microstructure evolution and grain boundary junction engineering *Mater. Sci. Technol.* **21** 1261–6

[43] Chellali M R, Balogh Z, Bouchikhaoui H, Schlesiger R, Stender P, Zheng L and Schmitz G 2012 Triple junction transport and the impact of grain boundary width in nanocrystalline Cu *Nano Lett.* **12** 3448–54

[44] Plimpton S 1995 Fast parallel algorithms for short-range molecular dynamics *J. Comput. Phys.* **117** 1–19

[45] Mishin Y, Mehl M J, Papaconstantopoulos D A, Voter A F and Kress J D 2001 Structural stability and lattice defects in copper: *ab initio*, tight-binding, and embedded-atom calculations *Phys. Rev. B* **63** 224106

[46] Nosé S 1984 A unified formulation of the constant temperature molecular dynamics methods *J. Chem. Phys.* **81** 511

[47] Hoover W G 1985 Canonical dynamics: equilibrium phase-space distributions *Phys. Rev. A* **31** 1695–7

[48] Janssens K G F, Olmsted D, Holm E A, Foiles S M, Plimpton S J and Derlet P M 2006 Computing the mobility of grain boundaries *Nature Mater.* **5** 124–7

[49] Homer E R, Foiles S M, Holm E A and Olmsted D L 2013 Phenomenology of shear-coupled grain boundary motion in symmetric tilt and general grain boundaries *Acta Mater.* **61** 1048–60

[50] Li J 2003 AtomEye: an efficient atomistic configuration viewer *Modelling Simul. Mater. Sci. Eng.* **11** 173

[51] Zhang H, Upmanyu M and Srolovitz D J 2005 Curvature driven grain boundary migration in aluminum: molecular dynamics simulations *Acta Mater.* **53** 79–86

[52] Upmanyu M, Smith R W and Srolovitz D J 1998 Atomistic simulation of curvature driven grain boundary migration *Interface Sci.* **6** 41–58

[53] Cahn J W, Mishin Y and Suzuki A 2006 Coupling grain boundary motion to shear deformation *Acta Mater.* **54** 4953–75

[54] Bernstein N 2008 The influence of geometry on grain boundary motion and rotation *Acta Mater.* **56** 1106–13

[55] Trautt Z T, Adland A, Karma A and Mishin Y 2012 Coupled motion of asymmetrical tilt grain boundaries: molecular dynamics and phase field srystal simulations *Acta Mater.* **60** 6528–46